iScience

CellPress
OPEN ACCESS

Article

Depletion of cardiac cardiolipin synthase alters systolic and diastolic function

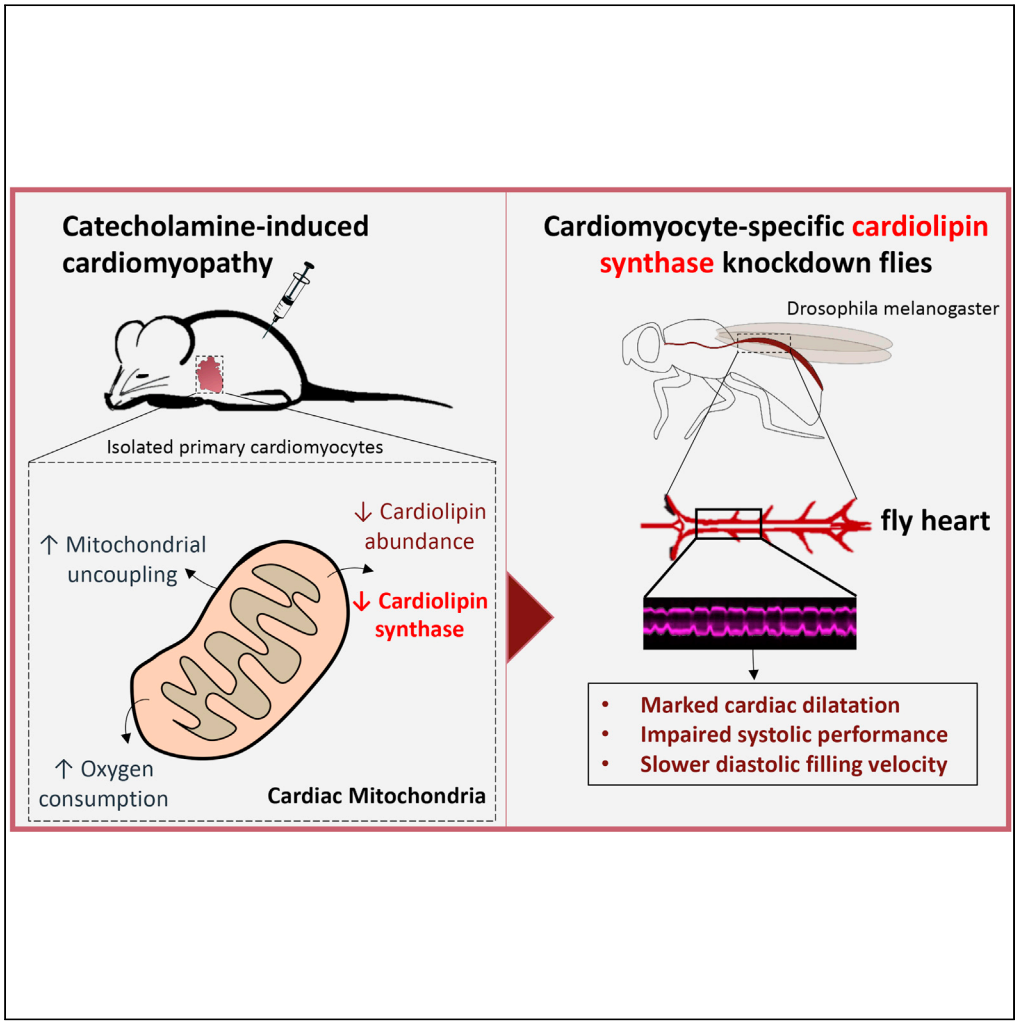

Elia Smeir, Sarah Leberer, Annelie Blumrich, ..., Rolf Bodmer, Anna Foryst-Ludwig, Ulrich Kintscher

ulrich.kintscher@charite.de

Highlights

Cardiolipin synthase (CLS) is reduced in isoproterenol (ISO)-induced cardiac damage

This is accompanied by alterations of cardiolipins and mitochondrial function

CLS mutant *Drosophila melanogaster* exhibit mild cardiac changes

Cardiomyocyte-CLS knockdown in *Drosophila* results in severe cardiac dysfunction

Smeir et al., iScience 24, 103314
November 19, 2021
https://doi.org/10.1016/j.isci.2021.103314

iScience

CellPress
OPEN ACCESS

Article

Depletion of cardiac cardiolipin synthase alters systolic and diastolic function

Elia Smeir,[1,2,9] Sarah Leberer,[1,2,9] Annelie Blumrich,[1,2] Georg Vogler,[3] Anastasia Vasiliades,[1,2] Sandra Dresen,[1,2] Carsten Jaeger,[4] Yoann Gloaguen,[5,6] Christian Klose,[7] Dieter Beule,[5] P. Christian Schulze,[8] Rolf Bodmer,[3] Anna Foryst-Ludwig,[1,2,9] and Ulrich Kintscher[1,2,9,10,*]

SUMMARY

Cardiolipin (CL) is a major cardiac mitochondrial phospholipid maintaining regular mitochondrial morphology and function in cardiomyocytes. Cardiac CL production includes its biosynthesis and a CL remodeling process. Here we studied the impact of CL biosynthesis and the enzyme cardiolipin synthase (CLS) on cardiac function. CLS and cardiac CL species were significantly downregulated in cardiomyocytes following catecholamine-induced cardiac damage in mice, accompanied by increased oxygen consumption rates, signs of oxidative stress, and mitochondrial uncoupling. RNAi-mediated cardiomyocyte-specific knockdown of CLS in *Drosophila melanogaster* resulted in marked cardiac dilatation, severe impairment of systolic performance, and slower diastolic filling velocity assessed by fluorescence-based heart imaging. Finally, we showed that CL72:8 is significantly decreased in cardiac samples from patients with heart failure with reduced ejection fraction (HFrEF). In summary, we identified CLS as a regulator of cardiac function. Considering the cardiac depletion of CL species in HFrEF, pharmacological targeting of CLS may be a promising therapeutic approach.

INTRODUCTION

Heart failure (HF) is a major health and economic burden with increasing prevalence in developed and developing countries (Crespo-Leiro et al., 2016). Despite significant advances in the last decades, recent therapeutic approaches for HF are insufficient to decrease its prevalence and to improve prognosis. HF is categorized depending on symptoms and clinical signs into two major forms, HF with reduced ejection fraction (HFrEF) or HF with preserved ejection fraction (HFpEF) (Ponikowski et al., 2016).

In HFrEF and HFpEF, mitochondrial dysfunction is a hallmark of pathogenesis (Bertero and Maack, 2018; Kumar et al., 2019). These alterations comprise structural and energetic abnormalities of cardiomyocyte mitochondria including an increased reactive oxygen species (ROS) production, altered mitochondrial Ca^{2+} handling, and impaired ATP production (Bertero and Maack, 2018; Kumar et al., 2019). Mitochondria consist of two membranes, an outer membrane and an inner membrane, which forms cristae structures and harbors the respiratory chain complexes (Murphy et al., 2016). Mitochondrial membranes are composed of multiple proteins and a distinct pool of phospholipids that maintain their structural integrity and function (Murphy et al., 2016).

Cardiolipin (CL) is one of the most important mitochondrial phospholipids, exclusively present in the inner mitochondrial membrane (Dudek et al., 2019). It plays a major role in maintaining mitochondrial morphology (e.g., membrane bending) and regulates mitochondrial fission and fusion (Dudek et al., 2019). CL depletion results in deterioration of mitochondrial respiration including a loss of respiratory chain supercomplexes and membrane potential, increased ROS production, and decreased ATP synthesis (Dudek et al., 2019). Accordingly, lower levels of cardiac CL have been described in preclinical models of cardiac damage, such as during ischemia, in spontaneously hypertensive HF rats, and in aging hearts (Lesnefsky et al., 2001; Pepe et al., 1999; Sparagna et al., 2005). Data in humans are rather limited showing a reduction of cardiac CL content in ischemic and dilated cardiomyopathy (Heerdt et al., 2002; Sparagna et al., 2005).

[1]Charite - Universitätsmedizin Berlin, Corporate Member of Freie Universität Berlin, Humboldt-Universität zu Berlin, and Berlin Institute of Health/ Institute of Pharmacology, Center for Cardiovascular Research, Hessische Street 3-4, 10115 Berlin, Germany

[2]DZHK (German Centre for Cardiovascular Research), Partner Site, Berlin, Germany

[3]Development, Aging and Regeneration Program, Sanford-Burnham-Prebys Medical Discovery Institute, La Jolla, CA 92037, USA

[4]Federal Institute for Materials Research and Testing (BAM), Berlin, Germany

[5]Berlin Institute of Health, BIH, Core Unit Bioinformatics, Berlin, Germany

[6]Berlin Institute of Health, BIH, Metabolomics Platform, Berlin, Germany

[7]Lipotype GmbH, Dresden, Germany

[8]Department of Internal Medicine I, Division of Cardiology, Angiology, Pneumology and Intensive Medical Care, University Hospital Jena, Friedrich-Schiller-University Jena, Jena, Germany

[9]These authors contributed equally

[10]Lead contact

*Correspondence: ulrich.kintscher@charite.de

https://doi.org/10.1016/j.isci.2021.103314

The most abundant CL species in the heart is tetralinoleoyl-CL (CL72:8) (Schlame and Greenberg, 2017). CL production takes place located in the inner mitochondrial membrane and involves its biosynthesis and a remodeling process in which the fatty acid composition is modified in a tissue-specific manner (Schlame and Greenberg, 2017). The CL-remodeling process, mediated by the enzyme tafazzin, has been well studied with regard to its impact on cardiac function (Schlame and Xu, 2020), whereas less data exist on the importance of enzymes involved in CL biosynthesis. Cardiolipin synthase (CLS) is one of the crucial enzymes in CL biosynthesis regulating the last step before nascent CL is remodeled to mature CL (Lu et al., 2006; Schlame and Hostetler, 1991). CLS transfers a phosphatidyl group from cytidine diphosphate (CDP) to phosphatidylglycerol (PG) catalyzing the synthesis of nascent CL (Schlame and Greenberg, 2017). The role of CLS in the regulation of cardiac function and in the development of HF is less well understood.

In this study, we analyzed cardiomyocytic CLS expression, CL species abundance, and mitochondrial function in a murine model of isoproterenol (ISO)-induced cardiac damage. To prove a causative link between alterations of CLS activity and cardiac contractile function, we investigated *Drosophila melanogaster* with mutated CLS, as well as flies with a cardiac-specific knockdown of CLS by RNA interference. Cardiac function in *Drosophila* was assessed, as recently described, using high-resolution video microscopy combined with a fluorescence-based approach in unanesthetized whole flies carrying the red fluorophore tdTomato under control of a cardiomyocyte-specific enhancer (Klassen et al., 2017). Finally, we analyzed the abundance of CL species in heart samples from patients with HFrEF and in control samples.

RESULTS

Lower abundance of cardiomyocytic CLs and CLS in catecholamine-induced cardiomyopathy

To study the regulation of CL metabolism in cardiomyocytes during the development of cardiac damage, we used the well-established model of catecholamine-induced cardiomyopathy, as previously described (Beyhoff et al., 2017, 2019). As a result of regional cardiac hypoxia, cell death including apoptosis and inflammation occur shortly after treatment with the synthetic catecholamine ISO (Beyhoff et al., 2017). In this study, we isolated primary cardiomyocytes (PCMs) shortly after a 4-day ISO application and performed mass spectrometry (MS)-based shotgun-lipidomic analysis (Figure 1A). Lipid species with at least three valid measurements in each group were included in the analysis. We detected 299 lipid species from 19 different lipid classes (Figure 1B and Tables S1 and S2). The most abundant lipid classes in PCMs were CLs, phosphatidylcholines, and phosphatidylethanolamines, among which only CLs were significantly downregulated in PCMs isolated from ISO-treated mice (Figure 1C and Table S2). Further analysis of the individual lipids revealed 24 significantly regulated lipid species between PCMs from vehicle- and ISO-treated mice (Figure 1D). Consistent with the lower abundance of the CL lipid class, four CL species were downregulated in the ISO group including CL72:8, CL72:9, CL74:8, and CL74:9 (Figure 1D). Interestingly, low levels of CL species in PCMs from ISO-treated mice were accompanied by significantly reduced expression levels of CLS suggesting a reduction of CL biosynthesis as a cause of diminished cardiac CLs (Figure 1E). This is further supported by an increase of multiple PG species, which are substrates of CLS, in the lipidomic analysis of PCMs from ISO-treated versus vehicle-treated mice (Figure 1D). In addition to CLs, two triacylglycerol (TAG) species (TAG 56:5, TAG 54:6) were significantly reduced by ISO (Figure 1D).

Lipid peroxidation and alterations of mitochondrial respiration under catecholamine-induced cardiac stress

Since the depletion of cardiac CLs has been accompanied by enhanced ROS production and mitochondrial dysfunction (Dudek et al., 2019), we wanted to know whether the reduction of CL species in our model associates with oxidative stress and changes in mitochondrial respiration. Serum malondialdehyde (MDA) levels, a robust marker of lipid peroxidation and oxidative stress, were significantly higher in ISO-treated mice, as assessed with the thiobarbituric acid reactive substances (TBARS) assay (Figure 2A). Mitochondrial respiration was assessed in PCMs using the Seahorse XF96e Analyzer combined with a mitochondrial stress test. Oxygen consumption measurements revealed a significant increase of maximal respiration and spare respiratory capacity in PCMs from ISO-treated mice (Figures 2B and 2C). In parallel, the respiratory control ratio, an indicator of mitochondrial coupling, tended to be lower in the ISO group, which was accompanied by increased expression of the uncoupling proteins, UCP2 and UCP3, in PCMs (Figures 2D and 2E). Finally, the extracellular acidification rate (ECAR), a marker of lactate production and glycolytic turnover (Divakaruni et al., 2014), was significantly higher in PCMs from ISO-treated mice compared with vehicle-controls (Figure 2F).

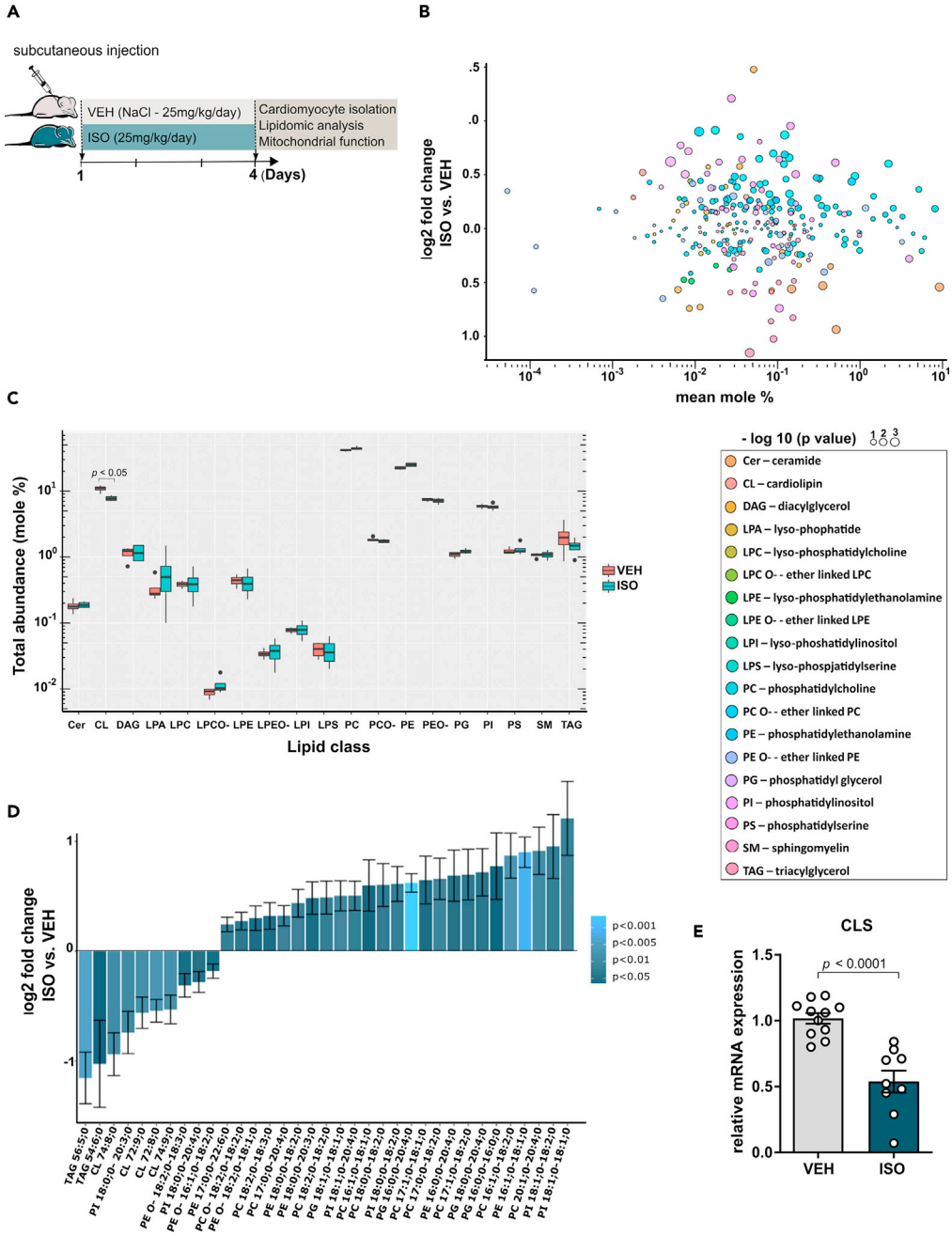

Figure 1. Lower abundance of cardiomyocytic CLs and CLS in catecholamine-induced cardiomyopathy

(A) Schematic overview of experimental setup: 8-week-old 129SV mice were subcutaneously injected with either NaCl (VEH) or isoproterenol (ISO) 25 mg/kg/day for 4 consecutive days; 2 h after last ISO injection, primary cardiomyocytes (PCMs) were isolated and used for indicated experiments.

(B) Scatterplot displays mean estimated log2-transformed fold change (ISO versus VEH PCMs) on the y axis and mean mole percent of lipid species on the x axis. Each bubble represents a single lipid species. VEH n = 4, ISO n = 5, t test, bubble size indicates -log10 p value.

(C) For each lipid class median, lower/upper quartile, min-max of total mole percent values are shown on a logarithmic scale; black dots indicate outliers. VEH n = 4, ISO n = 5, Wilcoxon test.

(D) Bar graphs showing the estimated log2-fold change (PCMs ISO versus VEH) ± regression standard error of differentially and significantly changed lipid species. VEH n = 4, ISO n = 5. Colors represent -log10 p values as indicated.

(E) mRNA expression of cardiolipin synthase (CLS) in PCMs from vehicle-treated (VEH) versus ISO-treated mice. n = 9–11 mice/group; data are shown as mean ± SEM, t test.

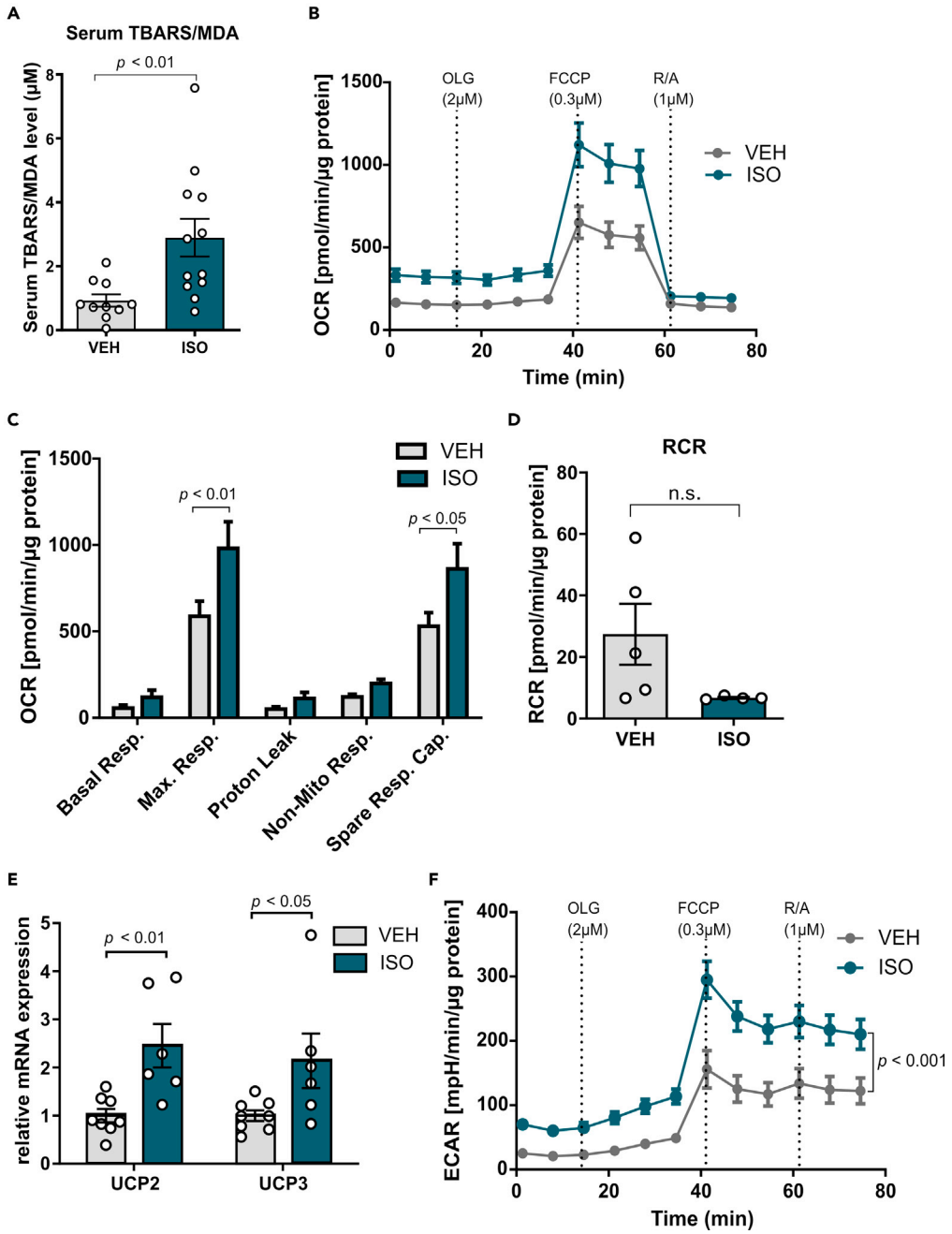

Figure 2. Lipid peroxidation and alterations of mitochondrial respiration under catecholamine-induced cardiac stress

(A) Serum levels of malondialdehyde (MDA) after 4 days ISO application assessed by the TBARS assay. n = 10–12 mice/group; data are shown as mean ± SEM, t test.

(B) Mitochondrial stress test using the Seahorse XFe96 Analyzer was performed with PCMs from ISO- and VEH-treated mice. Shown is the oxygen consumption rate (OCR) over time with application of oligomycin A (OLG), carbonyl cyanide-*p*-trifluoromethoxyphenylhydrazone (FCCP), and rotenone/antimycin A (R/A).

(C) OCR-based quantification (pmol/min/protein content in µg) of basal respiration, maximal respiration, proton leak, non-mitochondrial respiration, and spare respiratory capacity analyzed with the Seahorse XFe96 Analyzer in PCMs from ISO- and VEH-treated mice.

(D) Respiratory control rate (RCR = maximal respiration/proton leak) in PCMs from ISO- and VEH-treated mice.

Figure 2. *Continued*
(E) mRNA expression of uncoupling protein (UCP) 2 and 3 in PCMs from ISO- and VEH-treated mice.
(F) Extracellular acidification rate (ECAR) during mitochondrial stress test (application of OLG, FCCP, R/A) using the Seahorse XFe96 Analyzer. PCMs for Seahorse experiments were isolated from n = 4–5 mice/group, data are shown as mean ± SEM, two-way ANOVA with Sidak's multiple comparison test. qPCR data (E) are shown as mean ± SEM, t test.

Together these data demonstrate that low CL and TAG abundance in PCMs from ISO-mediated cardiomyopathy is associated with higher rates of mitochondrial respiration, enhanced oxidative stress, and signs of altered mitochondrial coupling.

Depletion of cardiac CLS results in systolic and diastolic dysfunction

To prove that reduced CLS expression, low CL levels, and mitochondrial alterations play a causal role in the development of cardiac dysfunction, we next used *Drosophila melanogaster*, an established genetic model in the analysis of cardiac physiology (Ocorr et al., 2014). Heart function in *Drosophila* was evaluated by a recently published fluorescence-based technique in unanesthetized whole flies carrying the red fluorophore tdTomato under control of a cardiomyocyte-specific enhancer (R94C02) (Figure 3A) (Klassen et al., 2017). Using this technique, we can assess cardiac diameters, fractional shortening, kinetics of contraction/relaxation, and parameters of the cardiac cycle such as heart rate and heart period (systolic and diastolic interval) (Figure 3A) (Klassen et al., 2017).

Mutations in the gene encoding CLS in *Drosophila* have been previously shown to result in a robust reduction of CL level, a compensatory increase of PGs, and mitochondrial dysfunction in whole flies (Acehan et al., 2011a), a phenotype that resembles the PCM phenotype in ISO-treated mice. In consonance with these data, we observed a marked decline of multiple CL species in CLS heterozygous mutant flies ($CLS^{-/+}$) compared with control wild-type flies (Figure 3B). Analysis of heart function in CLS mutant flies compared with control wild-type flies ($Ctrl^{w1118}$) revealed enlarged cardiac diameters (Figures 3C–3E), a reduced heart rate (Figure 3F), and unchanged fractional shortening (Figure 3G). In accordance with the reduced heart rate, we observed a prolonged heart period (Figure 3H), as well as extended systolic and diastolic intervals (Figures 3I and 3J), in CLS mutant flies. Maximal speed of contraction was slightly increased in CLS mutants (Figure 3K) whereas the maximal speed of relaxation was not affected (Figure 3L). Finally, CLS mutation resulted in a higher arrhythmia index (Figures 3M and 3N). These data suggest that a global reduction of CLS activity and CL levels in whole flies mediate a cardiac dysfunction with cardiac enlargement associated with a reduced heart rate and arrhythmias.

To determine whether the knockdown of CLS specifically in the heart alters cardiac function, the binary *UAS-GAL4* system with the cardiomyocyte-specific *Hand4.2-GAL4* driver combined with RNAi constructs against CLS was used. Flies with a specific knockdown of CLS in cardiomyocytes (Hand > CLS $RNAi^{KK}$) showed cardiac enlargement (Figures 4A–4C), reduced heart rate (Figure 4D), and impairment of systolic function with a dramatic reduction of fractional shortening (Figure 4E) compared with driver (Hand/$+^{KK}$) and RNAi (CLS $RNAi^{KK}$/+) control flies. Cardiac-specific CLS knockdown also resulted in a prolonged heart period (Figure 4F) with longer diastolic and unchanged systolic intervals (Figures 4G and 4H). In accordance with the impairment of fractional shortening, the kinetics of contraction (maximum speed of contraction) were altered in cardiac-specific CLS knockdown flies (Figure 4I). Surprisingly, this was accompanied by a decrease in the velocity of relaxation indicating the presence of diastolic dysfunction when cardiac CLS is reduced (Figure 4J). Finally, hearts from cardiac-specific CLS knockdown flies showed considerably more arrhythmic events, as demonstrated by an increased arrhythmia index, compared with control flies (Figures 4K and 4L).

To demonstrate a link between decreased CL level and the regulation of cardiac mitochondrial respiration, we analyzed the cardiac oxygen consumption rate using the Seahorse XFe Analyzer. *Drosophila* hearts from CLS heterozygous mutant flies ($CLS^{-/+}$) and control wild-type flies ($Ctrl^{w1118}$) were prepared, as previously described (Blumrich et al., 2021). We observed no significant differences in basal, maximal, and ATP-linked respiration between CLS mutant flies and control wild-type flies (Figures 5A and 5B). However, CLS mutant fly hearts exhibited a significantly enhanced proton leak and a reduced spare respiratory capacity (Figures 5A and 5B).

Together, cardiac-specific knockdown of CLS results in severe systolic and diastolic dysfunction accompanied by heart dilatation and arrhythmias.

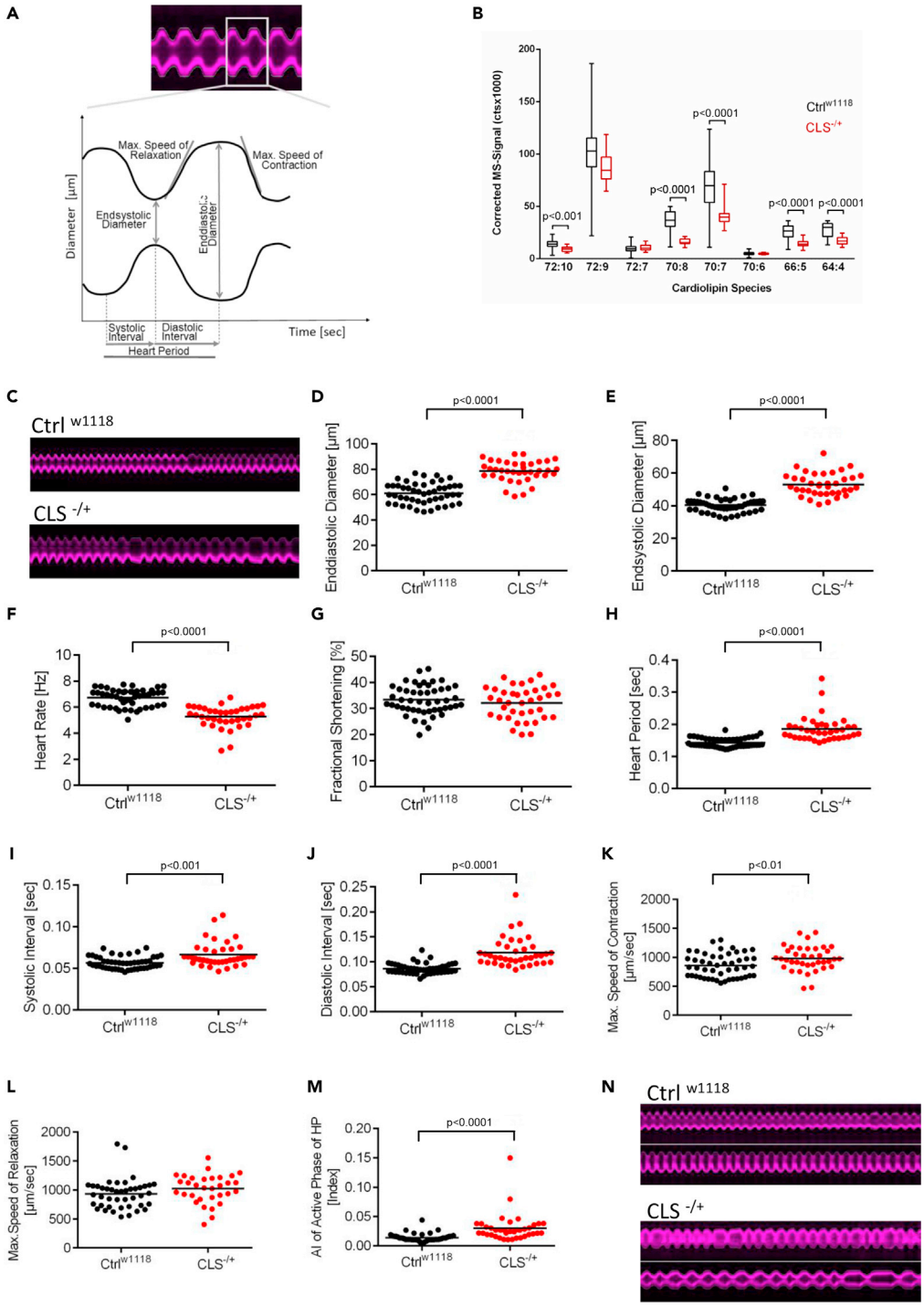

Figure 3. Cardiac performance in CLS mutants

(A) Representative images (upper part) of heart wall movement in control wild-type flies (Ctrl^{w1118}) using a fluorescence-based technique in unanesthetized whole flies carrying the red fluorophore tdTomato under control of a cardiomyocyte-specific enhancer (R94C02). Outline of analyzed cardiac performance parameters after digitization of fluorescence images.

(B) Lipid samples from whole flies (wild-type: Ctrl^{w1118} and CLS mutant: CLS$^{-/+}$) were analyzed by liquid chromatography-mass spectrometry (MS). Abundance of cardiolipin species is shown as MS signal intensity (n = 17–18, each sample contains a pool of three flies; data are shown as median, lower/upper quartile, and min-max; unpaired t test).

Figure 3. *Continued*
(C) Representative images of heart wall movement in control wild-type flies ($Ctrl^{w1118}$) and CLS mutants ($CLS^{-/+}$).
(D–N) Parameters of cardiac performance calculated from heart wall movement imaging as outlined in Figure 3A. AI: arrhythmia index. N = 3, n = 40/49 flies. Data are shown as mean, unpaired t test. (N) Representative images of arrhythmic events in control wild-type flies ($Ctrl^{w1118}$) and CLS mutants ($CLS^{-/+}$).

Cardiac CL levels are reduced in patients with HFrEF

To demonstrate the translational relevance of our observations in mice and flies for human pathology, we measured CL level in left ventricular (LV) samples from patients with HFrEF (n = 10; male/female [m/f]: 8/2; age [mean ± SD]: 52.8 ± 15.2 years) and control subjects (n = 5; m/f: 5/0; age [mean ± SD]: 51.2 ± 25.5 years) using a MS-based shotgun analysis. Patients with HFrEF had a LV-EF (ejection fraction) of 19% ± 5% (mean ± SD), and in all control subjects the LV-EF was normal (>60%). Within the HFrEF group, 8 patients were diagnosed with dilated cardiomyopathy and 2 patients with ischemic cardiomyopathy.

As depicted in Figure 6, several CL species tended to be lower in LV samples from patients with HFrEF, among which the most abundant CL species in the mammalian heart, tetralinoleoyl-CL (CL72:8), was significantly reduced. These data suggest that our observations in mice and flies appear to translate also to human HF, in which CL depletion may be a relevant disease contributing factor with a potential for therapeutic targeting.

DISCUSSION

In this study, we identified CLS, a key enzyme for the biosynthesis of mitochondrial CLs, as a regulator of cardiac function. CLS was downregulated in cardiomyocytes during catecholamine-induced cardiac damage in mice, associated with a significant decline of cardiac CL and TAG species, increased mitochondrial respiration, enhanced oxidative stress, and sign of mitochondrial uncoupling. Cardiomyocyte-specific knockdown of CLS in *Drosophila* resulted in cardiac dilatation, severe impairment of systolic performance, and diastolic dysfunction. These processes may play an important role in human HF since cardiac depletion of CL is present in HFrEF.

The production of mitochondrial CL involves its biosynthesis and a subsequent remodeling process (Schlame and Greenberg, 2017). CL remodeling is catalyzed by the enzyme tafazzin, which produces mature CL by reacylation of monolyso-CL (Schlame and Greenberg, 2017). Mutations in the tafazzin gene result in a reduction of the mature CL form and are closely related to the Barth syndrome, a genetic disease with cardiomyopathy and muscle weakness (Dudek et al., 2019; Schlame and Greenberg, 2017). The CL remodeling process by tafazzin has been well studied in the context of cardiac function, whereas the impact of CL biosynthesis is less understood (Dudek et al., 2019). CLS is one of the key enzymes in this pathway mediating the last step to synthesize premature CL (Schlame and Greenberg, 2017). Here we show a significant downregulation of CLS expression in cardiomyocytes from mice with catecholamine-mediated cardiac damage. These data are consistent with previously published results from Saini-Chohan and colleagues showing reduced CLS mRNA expression and activity in failing hearts from spontaneously hypertensive rats (Saini-Chohan et al., 2009). Kiebish and colleagues investigated the role of CLS for myocardial lipidomic flux and cardiac mitochondrial function by generating a transgenic mouse model with cardiomyocyte-specific overexpression of human CLS (Kiebish et al., 2012). They unequivocally demonstrated that CLS regulates the production of cardiac tetralinoleoyl-CL (CL72:8) (Kiebish et al., 2012). Interestingly, overexpression of CLS in cardiomyocytes also resulted in alterations of its key substrate, cardiac PG (Kiebish et al., 2012), a regulation we also observed in our model. Furthermore, CLS overexpression resulted in an overall reduction of substrate-stimulated mitochondrial respiration but improved coupling and increased complex III activity, whereas ATP production was not affected (Kiebish et al., 2012). Although we did not modify CLS activity directly in our mouse model, some of the mitochondrial alterations observed by Kiebish and colleagues correspond to the changes observed in catecholamine-stressed PCMs, in which CLS expression and CL species were significantly downregulated.

To the best of our knowledge, no study has yet investigated the direct impact of cardiac CLS on cardiac function. For this purpose, we analyzed the effects of CLS depletion on cardiac systolic and diastolic function in unanesthetized *Drosophila* using a new fluorescence-based technique for fly heart phenotyping. In previous studies, CLS mutant flies with CLS depletion in the whole fly, exhibited low levels of CLs, an increase of PGs, and a pronounced mitochondrial phenotype with diminished mitochondrial respiratory

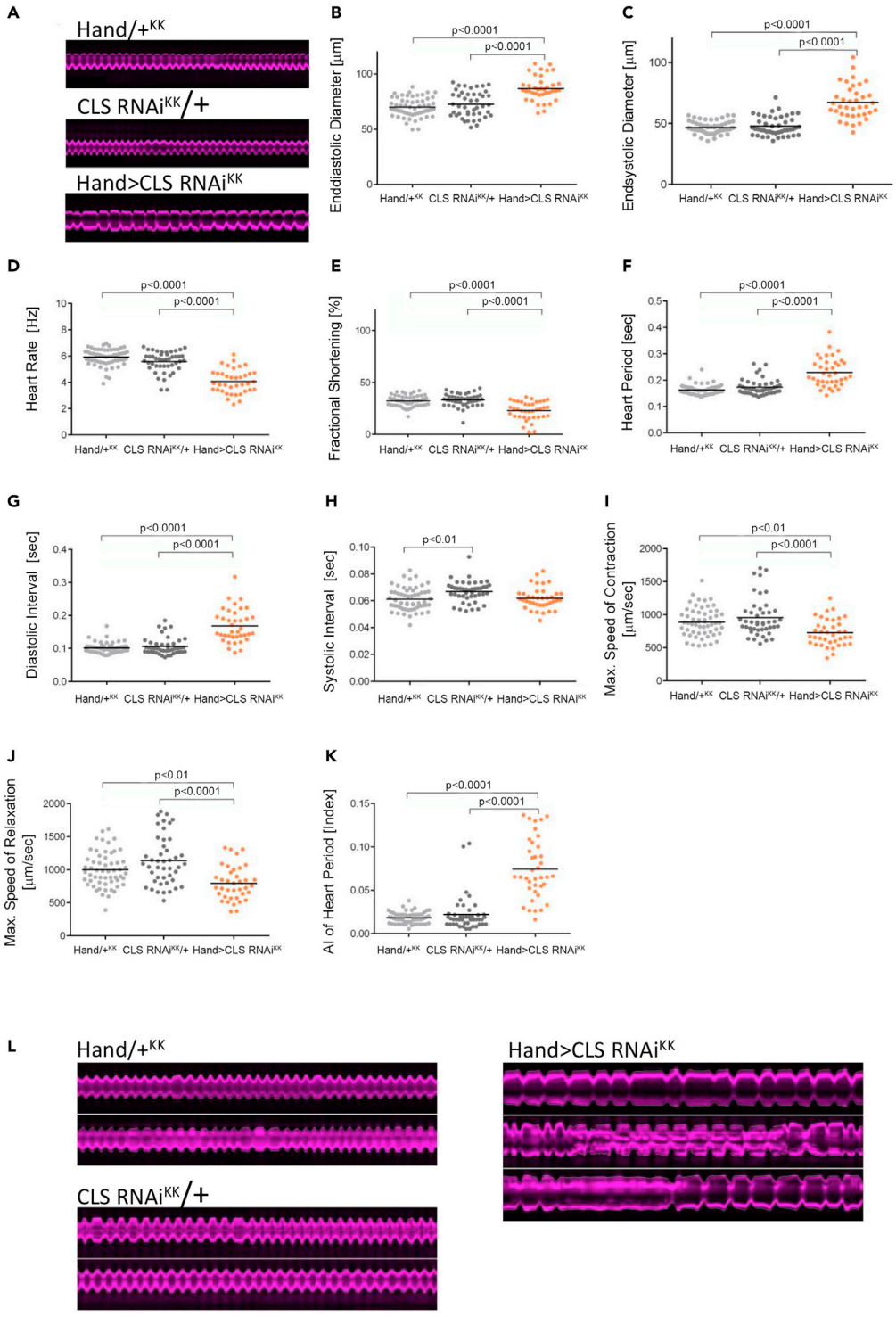

Figure 4. Cardiac performance in cardiac specific CLS knockdown flies

(A) Representative images of heart wall movement in control wild-type flies (Hand/+^{KK} and CLS RNAi^{KK}/+) and cardiomyocyte-specific CLS-RNAi knockdown flies (Hand > CLS RNAi^{KK}).

(B–K) Parameters of cardiac performance in control wild-type flies (Hand/+^{KK} and CLS RNAi^{KK}/+) and cardiomyocyte-specific CLS-RNAi knockdown flies (Hand > CLS RNAi^{KK}) calculated from heart wall movement imaging as outlined in

Figure 4. *Continued*
Figure 3A. AI: arrhythmia index. N = 4, n = 57/45/38 flies. Data are shown as mean, one-way ANOVA with Bonferroni multiple comparison test.
(L) Representative images of arrhythmic events in control wild-type flies (Hand/+^{KK} and CLS RNAi^{KK}/+) (left panels) and cardiomyocyte-specific CLS-RNAi knockdown flies (Hand > CLS RNAi^{KK}) (right panels).

activity and deteriorated supramolecular organization of ATP synthase (Acehan et al., 2011a). Hearts of the CLS mutant showed abnormal mitochondrial morphology and a lower heart rate (Acehan et al., 2011a). Cardiac function was not assessed in this study (Acehan et al., 2011a). A decline in heart rate together with alterations of cardiac intervals was also observed in CLS mutant flies in our study. In addition, we detected enlarged chamber diameters and more arrhythmic events in flies with mutated *CLS*. In contrast to Acehan et al. (2011a), we observed only a very mild mitochondrial respiratory phenotype in hearts from mutant flies. However, several differences exist between these studies. Acehan and colleagues studied mitochondrial respiration in mitochondria isolated from fly thoraces, in which flight muscle is the most abundant tissue (Acehan et al., 2011a), whereas we analyzed intact fly hearts. Furthermore, we used CLS heterozygous mutant flies (CLS$^{-/+}$) outcrossed to wild-type flies, which may have resulted in an incomplete loss of CLS and higher cardiac CL levels compared with Acehan et al. (2011a). The cardiac phenotype deteriorated markedly when we reduced CLS specifically in the fly heart. RNAi-mediated cardiomyocyte-specific knockdown of CLS resulted in severe systolic and diastolic dysfunction with cardiac enlargement. This phenotype resembles, at least in part, the cardiac morphology and function of aged tafazzin-deficient mice (Acehan et al., 2011b; Soustek et al., 2011). Short hairpin RNA-mediated tafazzin knockdown resulted in end-diastolic and end-systolic LV enlargement and a significant reduction of fractional shortening (FS) and EF in mice older than 7 months (Acehan et al., 2011b; Soustek et al., 2011). The loss of tafazzin leads to a pronounced reduction of cardiac tetralinoleoyl-CL (Acehan et al., 2011b; Soustek et al., 2011), as seen in our model with CLS depletion. A typical change occurring in the tafazzin knockdown mice, in contrast to CLS alterations, is an increase in monolyso-CL and a higher ratio of monolyso-CL-to-CL, which may also participate in the phenotype of these mice (Acehan et al., 2011b; Ren et al., 2019; Soustek et al., 2011). These CL changes in the inner mitochondrial membrane mediated by tafazzin or *CLS* depletion, lead to a destabilization of mitochondrial respiratory chain complexes, resulting in cardiac dysfunction (Dudek et al., 2016; Ren et al., 2019).

We aimed to connect the studies in primary mouse cardiomyocytes from ISO-treated mice with our experiments in hearts from *Drosophila melanogaster*. Despite the fact that we observed reduced cardiomyocytic CLS expression and CL concentrations in catecholamine-treated mice, which mirrors the data in CLS mutant flies, the mitochondrial respiratory phenotype did not reflect the phenotype in flies. In addition, these data do not exactly correspond to the effects that would be expected with reduced cardiac CL levels. In this regard, Acehan and colleagues clearly showed a diminished mitochondrial respiratory activity and deteriorated supramolecular organization of ATP synthase (Acehan et al., 2011a), whereby ISO treatment resulted in an increase in maximal respiration and spare respiratory capacity. These data suggest that ISO treatment may also induce other cardiac metabolic alterations, irrespective of the CL/CLS regulation, which explains this amplified mitochondrial respiration. In addition to the reduction of multiple cardiomyocytic CL species, the MS-based lipidomic analysis revealed a significant reduction of TAGs. Reduced levels of cardiac TAGs have been also previously reported in patients with HFrEF (Chokshi et al., 2012). Catecholamine stimulation induces lipolysis leading to an increase in cardiac FA availability for β-oxidation (Bertero and Maack, 2018; Kintscher et al., 2020). This would further result in increased acetyl-CoA level entering the Krebs cycle, and in parallel inhibiting glucose-derived pyruvate oxidation (Hue and Taegtmeyer, 2009). Pyruvate would then be converted to lactate finally leading to an increased ECAR, observed in our study. The reduced TAG level under ISO could therefore be a sign of increased cardiac lipolysis and fatty acid oxidation, which in turn would explain enhanced mitochondrial respiration. However, complementary to the enhanced respiration seen under ISO, we also showed that mitochondrial coupling tends to be reduced, which was accompanied by higher cardiac UCP 2 and UCP 3 expression levels, as well as oxidative stress. Together, these data suggest that concomitant to a fatty acid-mediated stimulation of mitochondrial respiration by ISO, mitochondrial function does not appear completely normal. This, in turn, might be a result of low CL level and other ISO-mediated actions and may contribute to the observed deterioration of cardiac function in this model (Beyhoff et al., 2017).

We finally assessed, in a translational approach, the CL species abundance in LV samples from patients with HFrEF and found that tretalinoleoyl-CL is also reduced in failing human hearts. These data corroborate the

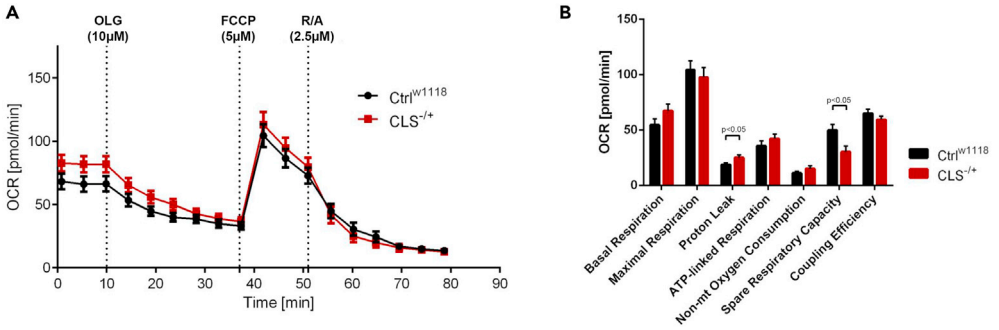

Figure 5. Mitochondrial respiration in hearts of CLS mutant flies

(A and B) Analysis of the oxygen consumption rate (OCR) over time with application of oligomycin A (OLG), carbonyl cyanide-*p*-trifluoromethoxyphenylhydrazone (FCCP), and rotenone/antimycin A (R/A) and (B) quantification of basal, maximal, and ATP-linked respiration, proton leak, non-mitochondrial (mt) oxygen consumption, spare respiratory capacity, and coupling efficiency from beating heart tubes of control ($Ctrl^{w1118}$) and heterozygous CLS mutant flies ($CLS^{-/+}$). (N = 2, n = 30 $Ctrl^{w1118}$, n = 31 $CLS^{-/+}$, mean ± SEM, unpaired t test.)

results previously published by other groups demonstrating that cardiac tetralinoleoyl CL is reduced in ischemic and dilated cardiomyopathy (Heerdt et al., 2002; Sparagna et al., 2007). Together these studies point toward a clinical relevance of cardiac CL depletion in HFrEF, which is further supported by recently developed drugs targeting CL in HF. Elamipretide is a cell-permeable tetrapeptide that targets the inner mitochondrial membrane, binds to CL, and improves cardiac mitochondrial function by yet largely unknown mechanisms (Sabbah et al., 2016). Despite promising pre-clinical results with elamipretide in HFrEF, a recently published clinical phase 2 study failed to prove a clear benefit of elamipretide in patients with HFrEF regarding changes of LV morphology and function assessed by cardiac magnetic resonance imaging (Butler et al., 2020). However, because the mechanism of elamipretide-mediated regulation of CL remains largely unknown at present, we believe that these data do not exclude the possibility that direct and specific pharmacological targeting of CLS or tafazzin may provide a benefit in HFrEF. Furthermore, studies on CL-based pharmacological intervention in HFpEF are currently ongoing.

Here we identify CLS as a regulator of cardiac function. These data in *Drosophila* suggest an important role of CLS in cardiac physiology and heart disease development. Further analyses of the pathophysiological significance of CLS in HFrEF and HFpEF should be performed in mammalian models, so that the pharmacological modification of this enzyme might then be used therapeutically.

Limitations of the study

Our study has distinct limitations. We showed that cardiac CLS knockdown in *Drosophila melanogaster* results in cardiac dysfunction, and we demonstrated reduced cardiomyocytic expression levels of CLS in a catecholamine-induced cardiac damage mouse model. However, we did not directly test the relevance of CLS and CLs in catecholamine-induced cardiac dysfunction. These experiments should be done in the future. CLS depletion in flies and mice likely affects cardiac function via mitochondrial dysfunction. Future experiments should assess mitochondrial function in hearts from CLS-deficient flies or mice and should directly link this to cardiac performance. In addition, the importance of the reduced levels of cardiac TAG under catecholamine treatment require further investigations. Finally, we could only assess cardiac CL levels in a small patient group with HFrEF. This analysis should be extended to other types of cardiac disease and should be connected to the cardiac energy status in humans.

STAR★METHODS

Detailed methods are provided in the online version of this paper and include the following:

- KEY RESOURCES TABLE
- RESOURCE AVAILABILITY
  - Lead contact
  - Materials availability
  - Data and code availability

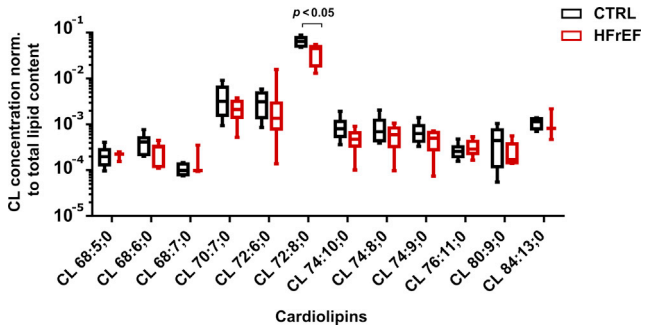

Figure 6. Cardiac CL levels are reduced in patients with HFrEF Cardiolipin (CL) species concentration in left ventricular myocardial samples normalized to total lipid content

Cardiac samples from HFrEF (n = 10) and control subjects (Ctrl) (n = 5) were subjected to MS-based shotgun analysis. Data are shown as median, lower/upper quartile, min-max; Mann-Whitney U test.

SUPPLEMENTAL INFORMATION

Supplemental information can be found online at https://doi.org/10.1016/j.isci.2021.103314.

ACKNOWLEDGMENTS

We thank Beata Hoeft for their excellent technical assistance. *Drosophila* stocks obtained from the Bloomington Drosophila Stock Center (NIH P40OD018537) were used in this study. Parts of this study were used in the PhD thesis of E.S., and will be used in the MD thesis of S.L. This study was supported by the Bundesinstitut für Risikobewertung (BfR) (BfR1328-564), the German Centre for Cardiovascular Research (DZHK) BER 5.4 PR, and the Deutsche Forschungsgemeinschaft (DFG – KI 712/10-1). E.S. is supported by the DZHK; BER 5.4 PR. U.K. is supported by the DZHK; BER 5.4 PR, the Deutsche Forschungsgemeinschaft (DFG - KI 712/10-1), the BfR1328-564, and the Einstein Foundation/Foundation Charité (EVF-BIH-2018-440). R.B. is supported by grants R01 HL54732 and P01 AG033456 from NIH.

AUTHOR CONTRIBUTIONS

E.S. and S.L. substantially contributed to conception and design of the study, acquisition of data, and data analysis and interpretation; drafted the article; and revised the article critically for important intellectual content. A.B. contributed to conception and design of the study and data analysis and interpretation and revised the article critically. G.V. substantially contributed to conception and design of the study and data analysis and interpretation and revised the article critically. A.V. and S.D. contributed to data acquisition, analysis, and interpretation and revised the article critically. C.J. substantially contributed to conception of the study, acquisition of data, and data analysis and interpretation (MS analysis). Y.G. and D.B. substantially contributed to data analysis and interpretation and revised the article critically. C.K. contributed to conception of the study and data analysis and interpretation and revised the article critically. P.C.S. contributed to conception of the study, acquisition of data, and data analysis and interpretation (human study) and revised the article critically. R.B. and A.F.-L. substantially contributed to conception and

design of the study and data analysis and interpretation and revised the article critically for important intellectual content. U.K. substantially contributed to conception and design of the study and data analysis and interpretation; drafted the article; revised the article critically for important intellectual content; and substantially contributed to acquisition of funding. All authors finally approved the version to be published.

DECLARATION OF INTERESTS

C.K. is an employee of Lipotype GmbH, Dresden, Germany. All other authors have declared that no conflict of interest exists.

Received: April 14, 2021
Revised: September 13, 2021
Accepted: October 18, 2021
Published: November 19, 2021

REFERENCES

Acehan, D., Malhotra, A., Xu, Y., Ren, M., Stokes, D.L., and Schlame, M. (2011a). Cardiolipin affects the supramolecular organization of ATP synthase in mitochondria. Biophys. J. *100*, 2184–2192.

Acehan, D., Vaz, F., Houtkooper, R.H., James, J., Moore, V., Tokunaga, C., Kulik, W., Wansapura, J., Toth, M.J., Strauss, A., et al. (2011b). Cardiac and skeletal muscle defects in a mouse model of human Barth syndrome. J. Biol. Chem. *286*, 899–908.

Bell, R.M., Mocanu, M.M., and Yellon, D.M. (2011). Retrograde heart perfusion: the Langendorff technique of isolated heart perfusion. J. Mol. Cell. Cardiol. *50*, 940–950.

Bertero, E., and Maack, C. (2018). Metabolic remodelling in heart failure. Nat. Rev. Cardiol. *15*, 457–470.

Beyhoff, N., Brix, S., Betz, I.R., Klopfleisch, R., Foryst-Ludwig, A., Krannich, A., Stawowy, P., Knebel, F., Grune, J., and Kintscher, U. (2017). Application of speckle-tracking echocardiography in an experimental model of isolated subendocardial damage. J. Am. Soc. Echocardiogr. *30*, 1239–1250.e1232.

Beyhoff, N., Lohr, D., Foryst-Ludwig, A., Klopfleisch, R., Brix, S., Grune, J., Thiele, A., Erfinanda, L., Tabuchi, A., Kuebler, W.M., et al. (2019). Characterization of myocardial microstructure and function in an experimental model of isolated subendocardial damage. Hypertension *74*, 295–304.

Blumrich, A., Vogler, G., Dresen, S., Diop, S.B., Jaeger, C., Leberer, S., Grune, J., Wirth, E.K., Hoeft, B., Renko, K., et al. (2021). Fat-body brummer lipase determines survival and cardiac function during starvation in Drosophila melanogaster. iScience *24*, 102288.

Butler, J., Khan, M.S., Anker, S.D., Fonarow, G.C., Kim, R.J., Nodari, S., O'Connor, C.M., Pieske, B., Pieske-Kraigher, E., Sabbah, H.N., et al. (2020). Effects of elamipretide on left ventricular function in patients with heart failure with reduced ejection fraction: the PROGRESS-HF phase 2 trial. J. Card. Fail. *26*, 429–437.

Chokshi, A., Drosatos, K., Cheema, F.H., Ji, R., Khawaja, T., Yu, S., Kato, T., Khan, R., Takayama, H., Knoll, R., et al. (2012). Ventricular assist device implantation corrects myocardial lipotoxicity, reverses insulin resistance, and normalizes cardiac metabolism in patients with advanced heart failure. Circulation *125*, 2844–2853.

Crespo-Leiro, M.G., Anker, S.D., Maggioni, A.P., Coats, A.J., Filippatos, G., Ruschitzka, F., Ferrari, R., Piepoli, M.F., Delgado Jimenez, J.F., Metra, M., et al. (2016). European society of cardiology heart failure long-term registry (ESC-HF-LT): 1-year follow-up outcomes and differences across regions. Eur. J. Heart Fail. *18*, 613–625.

Divakaruni, A.S., Paradyse, A., Ferrick, D.A., Murphy, A.N., and Jastroch, M. (2014). Analysis and interpretation of microplate-based oxygen consumption and pH data. Methods Enzymol. *547*, 309–354.

Dudek, J., Cheng, I.F., Chowdhury, A., Wozny, K., Balleininger, M., Reinhold, R., Grunau, S., Callegari, S., Toischer, K., Wanders, R.J., et al. (2016). Cardiac-specific succinate dehydrogenase deficiency in Barth syndrome. EMBO Mol. Med. *8*, 139–154.

Dudek, J., Hartmann, M., and Rehling, P. (2019). The role of mitochondrial cardiolipin in heart function and its implication in cardiac disease. Biochim. Biophys. Acta Mol. Basis Dis. *1865*, 810–821.

Ejsing, C.S., Sampaio, J.L., Surendranath, V., Duchoslav, E., Ekroos, K., Klemm, R.W., Simons, K., and Shevchenko, A. (2009). Global analysis of the yeast lipidome by quantitative shotgun mass spectrometry. Proc. Natl. Acad. Sci. U S A *106*, 2136–2141.

Fink, M., Callol-Massot, C., Chu, A., Ruiz-Lozano, P., Izpisua Belmonte, J.C., Giles, W., Bodmer, R., and Ocorr, K. (2009). A new method for detection and quantification of heartbeat parameters in Drosophila, zebrafish, and embryonic mouse hearts. Biotechniques *46*, 101–113.

Heerdt, P.M., Schlame, M., Jehle, R., Barbone, A., Burkhoff, D., and Blanck, T.J. (2002). Disease-specific remodeling of cardiac mitochondria after a left ventricular assist device. Ann. Thorac. Surg. *73*, 1216–1221.

Herzog, R., Schuhmann, K., Schwudke, D., Sampaio, J.L., Bornstein, S.R., Schroeder, M., and Shevchenko, A. (2012). LipidXplorer: a software for consensual cross-platform lipidomics. PLoS One *7*, e29851.

Hue, L., and Taegtmeyer, H. (2009). The Randle cycle revisited: a new head for an old hat. Am. J. Physiol. Endocrinol. Metab. *297*, E578–E591.

Jaeger, C., and Lisec, J. (2018). Statistical and multivariate analysis of MS-based plant metabolomics data. Methods Mol. Biol. *1778*, 285–296.

Ji, R., Akashi, H., Drosatos, K., Liao, X., Jiang, H., Kennel, P.J., Brunjes, D.L., Castillero, E., Zhang, X., Deng, L.Y., et al. (2017). Increased de novo ceramide synthesis and accumulation in failing myocardium. JCI Insight *2*, e82922.

Kiebish, M.A., Yang, K., Sims, H.F., Jenkins, C.M., Liu, X., Mancuso, D.J., Zhao, Z., Guan, S., Abendschein, D.R., Han, X., et al. (2012). Myocardial regulation of lipidomic flux by cardiolipin synthase: setting the beat for bioenergetic efficiency. J. Biol. Chem. *287*, 25086–25097.

Kintscher, U., Foryst-Ludwig, A., Haemmerle, G., and Zechner, R. (2020). The role of adipose triglyceride lipase and cytosolic lipolysis in cardiac function and heart failure. Cell Rep. Med. *1*, 100001.

Klassen, M.P., Peters, C.J., Zhou, S., Williams, H.H., Jan, L.Y., and Jan, Y.N. (2017). Age-dependent diastolic heart failure in an in vivo Drosophila model. Elife *6*, e20851.

Kumar, A.A., Kelly, D.P., and Chirinos, J.A. (2019). Mitochondrial dysfunction in heart failure with preserved ejection fraction. Circulation *139*, 1435–1450.

Lesnefsky, E.J., Slabe, T.J., Stoll, M.S., Minkler, P.E., and Hoppel, C.L. (2001). Myocardial ischemia selectively depletes cardiolipin in rabbit heart subsarcolemmal mitochondria. Am. J. Physiol. Heart Circ. Physiol. *280*, H2770–H2778.

Livak, K.J., and Schmittgen, T.D. (2001). Analysis of relative gene expression data using real-time quantitative PCR and the 2(-Delta Delta C(T)) Method. Methods *25*, 402–408.

Lu, B., Xu, F.Y., Jiang, Y.J., Choy, P.C., Hatch, G.M., Grunfeld, C., and Feingold, K.R. (2006). Cloning and characterization of a cDNA encoding human cardiolipin synthase (hCLS1). J. Lipid Res. *47*, 1140–1145.

Murphy, E., Ardehali, H., Balaban, R.S., DiLisa, F., Dorn, G.W., 2nd, Kitsis, R.N., Otsu, K., Ping, P., Rizzuto, R., Sack, M.N., et al. (2016). Mitochondrial function, biology, and role in disease: a scientific statement from the american heart association. Circ. Res. *118*, 1960–1991.

Neville, K.E., Bosse, T.L., Klekos, M., Mills, J.F., Weicksel, S.E., Waters, J.S., and Tipping, M. (2018). A novel ex vivo method for measuring whole brain metabolism in model systems. J. Neurosci. Methods *296*, 32–43.

Ocorr, K., Vogler, G., and Bodmer, R. (2014). Methods to assess Drosophila heart development, function and aging. Methods *68*, 265–272.

Pepe, S., Tsuchiya, N., Lakatta, E.G., and Hansford, R.G. (1999). PUFA and aging modulate cardiac mitochondrial membrane lipid composition and Ca2+ activation of PDH. Am. J. Physiol. *276*, H149–H158.

Ponikowski, P., Voors, A.A., Anker, S.D., Bueno, H., Cleland, J.G., Coats, A.J., Falk, V., Gonzalez-Juanatey, J.R., Harjola, V.P., Jankowska, E.A., et al. (2016). 2016 ESC guidelines for the diagnosis and treatment of acute and chronic heart failure: the task force for the diagnosis and treatment of acute and chronic heart failure of the European Society of Cardiology (ESC) Developed with the special contribution of the Heart Failure Association (HFA) of the ESC. Eur. Heart J. *37*, 2129–2200.

Ren, M., Miller, P.C., Schlame, M., and Phoon, C.K.L. (2019). A critical appraisal of the tafazzin knockdown mouse model of Barth syndrome: what have we learned about pathogenesis and potential treatments? Am. J. Physiol. Heart Circ. Physiol. *317*, H1183–H1193.

Sabbah, H.N., Gupta, R.C., Kohli, S., Wang, M., Hachem, S., and Zhang, K. (2016). Chronic Therapy with elamipretide (MTP-131), a novel mitochondria-targeting peptide, improves left ventricular and mitochondrial function in dogs with advanced heart failure. Circ. Heart Fail. *9*, e002206.

Saini-Chohan, H.K., Holmes, M.G., Chicco, A.J., Taylor, W.A., Moore, R.L., McCune, S.A., Hickson-Bick, D.L., Hatch, G.M., and Sparagna, G.C. (2009). Cardiolipin biosynthesis and remodeling enzymes are altered during development of heart failure. J. Lipid Res. *50*, 1600–1608.

Salatzki, J., Foryst-Ludwig, A., Bentele, K., Blumrich, A., Smeir, E., Ban, Z., Brix, S., Grune, J., Beyhoff, N., Klopfleisch, R., et al. (2018). Adipose tissue ATGL modifies the cardiac lipidome in pressure-overload-induced left ventricular failure. PLoS Genet. *14*, e1007171.

Sampaio, J.L., Gerl, M.J., Klose, C., Ejsing, C.S., Beug, H., Simons, K., and Shevchenko, A. (2011). Membrane lipidome of an epithelial cell line. Proc. Natl. Acad. Sci. U S A *108*, 1903–1907.

Schlame, M., and Greenberg, M.L. (2017). Biosynthesis, remodeling and turnover of mitochondrial cardiolipin. Biochim. Biophys. Acta Mol. Cell. Biol. Lipids *1862*, 3–7.

Schlame, M., and Hostetler, K.Y. (1991). Solubilization, purification, and characterization of cardiolipin synthase from rat liver mitochondria. Demonstration of its phospholipid requirement. J. Biol. Chem. *266*, 22398–22403.

Schlame, M., and Xu, Y. (2020). The function of tafazzin, a mitochondrial phospholipid-lysophospholipid acyltransferase. J. Mol. Biol. *432*, 5043–5051.

Singleton, K., and Woodruff, R.I. (1994). The osmolarity of adult Drosophila hemolymph and its effect on oocyte-nurse cell electrical polarity. Dev. Biol. *161*, 154–167.

Soustek, M.S., Falk, D.J., Mah, C.S., Toth, M.J., Schlame, M., Lewin, A.S., and Byrne, B.J. (2011). Characterization of a transgenic short hairpin RNA-induced murine model of Tafazzin deficiency. Hum. Gene Ther. *22*, 865–871.

Sparagna, G.C., Chicco, A.J., Murphy, R.C., Bristow, M.R., Johnson, C.A., Rees, M.L., Maxey, M.L., McCune, S.A., and Moore, R.L. (2007). Loss of cardiac tetralinoleoyl cardiolipin in human and experimental heart failure. J. Lipid Res. *48*, 1559–1570.

Sparagna, G.C., Johnson, C.A., McCune, S.A., Moore, R.L., and Murphy, R.C. (2005). Quantitation of cardiolipin molecular species in spontaneously hypertensive heart failure rats using electrospray ionization mass spectrometry. J. Lipid Res. *46*, 1196–1204.

Surma, M.A., Herzog, R., Vasilj, A., Klose, C., Christinat, N., Morin-Rivron, D., Simons, K., Masoodi, M., and Sampaio, J.L. (2015). An automated shotgun lipidomics platform for high throughput, comprehensive, and quantitative analysis of blood plasma intact lipids. Eur. J. Lipid Sci. Technol. *117*, 1540–1549.

Tsugawa, H., Cajka, T., Kind, T., Ma, Y., Higgins, B., Ikeda, K., Kanazawa, M., VanderGheynst, J., Fiehn, O., and Arita, M. (2015). MS-DIAL: data-independent MS/MS deconvolution for comprehensive metabolome analysis. Nat. Methods *12*, 523–526.

Wang, J.W., Wong, A.M., Flores, J., Vosshall, L.B., and Axel, R. (2003). Two-photon calcium imaging reveals an odor-evoked map of activity in the fly brain. Cell *112*, 271–282.

STAR★METHODS

KEY RESOURCES TABLE

REAGENT or RESOURCE	SOURCE	IDENTIFIER
Biological samples		
Human myocardial specimen: Myocardial specimens from HFrEF patients & control subjects	Tissue bank at the University Hospital Jena, Germany/ Columbia University, NY, USA	N/A
Chemicals, peptides, and recombinant proteins		
Isoproterenol hydrochloride	Sigma-Aldrich	I6504-500 mg
Carbonyl cyanide-p-trifluoromethoxyphenylhydrazone (FCCP) Oligomycin Rotenone / Antimycin A	Agilent Technologies	103010-100
Heparin	Ratiopharm	
Collagenase, Type 2	Worthington Biochemical Corporation	LS004174
Laminin		
PBS	Gibco	14190-094
Ethanol	Merck	CAS 64-17-5
Claycomb medium	Sigma-Aldrich	# 51800C
dNTPs	Promega	U1511
M-MLV RT 5x Buffer	Promega	M5313
Random primer	Promega	C1181
Power SYBR green PCR mix	Thermofisher	4367659
XF base media	Agilent Technologies	# 103575 – 100
Penicilin/Streptomycin	Pan Biotech	P-0607100
2,3-Butanedione monoxime (BDM)	Sigma-Aldrich	B0753-100G
Fibronectin	Sigma-Aldrich	F1141-5MG
Gelatine from bovine skin	Sigma-Aldrich	9000-70-8
L-Glutamine	Sigma-Aldrich	G7513-100
Proteinase K	Invitek	N/A
RNase ZAP	Sigma-Aldrich	R2020-250ML
RNAsin	Promega	N2511
XF Calibrant	Agilent Technologies	100840-000
Fetal Bovine Serum	Merck	TMS-016-B
Trypsin/EDTA	Pan Biotech	P10-023-100
Sodium chloride (NaCl)	Merck	7647-14-5
Sodium Pyruvate	Sigma-Aldrich	P4562-5G
AlbuMAX™	Thermo Fischer Scientific	11020039
Antimycin	Sigma-Aldrich	A8674
DMEM	Sigma-Aldrich	D5030
ESI(+) Tune Mix	Sigma-Aldrich	00036
FCCP	Sigma-Aldrich	C2920
Oligomycin A	Sigma-Aldrich	75351
Rotenone	Sigma-Aldrich	R8875
Formula 4-24®	Carolina Biological Supply Company	173200
FlyNap®	Carolina Biological Supply Company	173010
Vaseline	Fagron	4979239

(*Continued on next page*)

Continued

REAGENT or RESOURCE	SOURCE	IDENTIFIER
Critical commercial assays		
Thiobarbituric Acid Reactive Substances (TBARS) TCA Method Assay Kit	Cayman Chemical	700870
Seahorse XFp Cell Mito Stress Test Kit	Agilent Technologies	103010-100
RNeasy Micro Kit	Qiagen	Cat # 74004
Experimental models: Organisms/strains		
Mouse:		
128/SV wild type mice	Janvier Labs	
Drosophila melanogaster:		
w1118;PBac{w[+mC]=PB}CLS[c01874]/TM6B, Tb]	Bloomington *Drosophila* Stock Center	BDSC ID #10741
w1118	Bloomington *Drosophila* Stock Center	BDSC ID #5905
Hand4.2-Gal4/(CyO); tdTomatoe attP2 W;;tdTomatoe attP2	Working Group Rolf Bodmer	N/A
CLS RNAi (KK, Chr 2)	Vienna *Drosophila* Resource Center	VDRC ID #108392
$w1118^{KK}$		VDRC ID # 60101
For fluorescence-based heart function analysis *Drosophila were crossed to td-Tomatoe (tdtK) flies* CLS mutant flies (BL #10741) were crossed to flies with td-Tomatoe (tdtK)-background. For heart specific CLS knockdown, UAS-CLS RNAi KK (VDRC #108392) flies were crossed to Hand4.2-Gal4; tdtK (Hand>CLS $RNAi^{KK}$).	N/A	N/A
Software and algorithms		
GraphPad Prism	Prism	N/A
R	https://rstudio.com/ https://github.com/gvogler/FlyHearts-tdtK-Rscripts	N/A
Biorad CFX Connect Software	https://www.bio-rad.com/	N/A
Inkscape	https://inkscape.org/de/	N/A
Lipotype Zoom	N/A	N/A
Wave Controller	https://www.agilent.com/	N/A
Zotero	https://www.zotero.org/	N/A

RESOURCE AVAILABILITY

Lead contact

Further information and requests for resources and reagents should be directed to and will be fulfilled by the lead contact, Dr. Anna Foryst-Ludwig (anna.foryst@charite.de)

Materials availability

Available through lead contact.

Data and code availability

- Lipidomics data from Figure 1 are available as Table S1. All other data reported in this paper will be shared by the lead contact upon request.
- This paper does not report original code.
- Any additional information required to reanalyze the data reported in this paper is available from the lead contact upon request

EXPERIMENTAL MODEL AND SUBJECT DETAILS

Mice were housed under constant environmental conditions and in a temperature-controlled facility (20-24°C), 55 ± 10% relative humidity with a 12-h:12-h light-dark cycle and fed ad libitum with a standard

diet (Salatzki et al., 2018). 7-9 weeks old 128/SV male wild type mice (Janvier Labs, France) were used throughout the studies.

Drosophila melanogaster were kept at room temperature in a 12 h light-dark cycle receiving standardized food (Formula 4-24®, Carolina, NC, USA). For experiments, three-week-old males were used.

METHOD DETAILS

Adult primary murine cardiomyocyte isolation

Mice were subcutaneously injected with ISO (n = 4–11) (25mg/kg body weight, dissolved in saline) or saline (VEH) (n = 5–10) for 4 consecutive days. Sample sizes are indicated in each figure legend. On day 4, two hours after the final injection, mice received an intraperitoneal injection of heparin (500 IE) and 10min later, mice were anesthetized by isoflurane and sacrificed by cervical dislocation. Mice were sacrificed at this time point to assess the acute effects of ISO on cardiomyocyte metabolism. Hearts were removed and the aorta was sheathed onto a cannula and mounted onto a Langendorff perfusion apparatus. Hearts were perfused retrograde for 10min with Ca^{2+}- free perfusion buffer and then with perfusion buffer containing 1250 Units Collagenase Type 2 (Worthington, NJ, USA) per liter and 0.01mM Ca^{2+} until the heart is pale and flaccid. Hearts were then cut off the cannula, minced, and filtered through a 140μm nylon net filter (Merck Millipore, Germany) and then Ca^{2+}-free perfusion buffer containing 10% Fetal Bovine Serum was added to neutralize the protease activity and then centrifuged for 1min at 500 rounds per minute at room temperature (Bell et al., 2011). Lastly, cells were gravity-sedimented through 3 Ca^{2+} gradients in a 15ml flacon at 37°C. The supernatant was removed and the pellets were re-suspended in perfusion buffer lacking BDM but containing incrementally increased Ca^{2+} concentrations (0.1mM Ca^{2+}; 0.5mM Ca^{2+}; 1mM Ca^{2+}) (Bell et al., 2011). After 10min the Ca^{2+} solution was aspirated and the pelleted cells were gently suspended in the subsequent Ca^{2+} gradient (Bell et al., 2011). Lastly, isolated PCMs were centrifuged, and the pellets were either re-suspended with Claycomb medium for further assays or frozen at −80°C for RNA analysis or re-suspended in PBS and stored in −80°C for lipidomic analysis.

MS-based lipidomic and CL-analysis

The MS-based lipidomic analysis of PCMs isolated from VEH- and ISO-treated mice, and human samples was conducted in cooperation with Lipotype GmbH (Dresden, Germany). Lipid extraction and analysis of PCMs were performed (Ejsing et al., 2009; Salatzki et al., 2018; Sampaio et al., 2011; Surma et al., 2015). Lipids were extracted using a two-step chloroform/methanol procedure (Ejsing et al., 2009). Samples were spiked with a 13 internal lipid standard mixture (Salatzki et al., 2018). After extraction, the organic phase was transferred to an infusion plate and dried in a speed vacuum concentrator followed by resuspension of dry extracts (Salatzki et al., 2018). All liquid handling steps were performed using Hamilton Robotics STARlet robotic platform with the Anti Droplet Control feature for organic solvents pipetting (Salatzki et al., 2018).

Samples were analyzed by direct infusion on a QExactive mass spectrometer (Thermo Fisher Scientific, MA, USA) equipped with a TriVersa NanoMate ion source (Advion Biosciences, NY, USA). Samples were analyzed in both positive and negative ion modes, as described (Salatzki et al., 2018). Both MS and MSMS data were combined to monitor CE, DAG and TAG ions as ammonium adducts; PC, PC O-, as acetate adducts; and CL, PA, PE, PE O-, PG, PI and PS as deprotonated anions (Salatzki et al., 2018). MS only was used to monitor LPA, LPE, LPE O-, LPI and LPS as deprotonated anions; Cer, HexCer, SM, LPC and LPC O- as acetate adducts. Data were analyzed with in-house developed lipid identification software based on LipidXplorer (Herzog et al., 2012; Salatzki et al., 2018). Only lipid identifications with a signal-to-noise ratio >5, and a signal intensity 5-fold higher than in corresponding blank samples were considered for further data analysis (Salatzki et al., 2018).

To perform cardiolipin analysis in *Drosophila*, three-week-old male flies were flash-frozen in liquid nitrogen and homogenized in groups of three using 300μl ice-cold 75% methanol. 750 μl methyl tert-butyl ether was added. Samples were shaken for 10min. Next, 175μl UPLC-H2O were added, followed by an incubation period of 10min. Samples were mixed and then centrifuged. Two times 100μl of the upper phase was taken and dried in a vacuum centrifuge. Afterwards lipid extracts were reconstituted. For cardiolipin determination, aliquots were analyzed by LC-MS. Samples were injected into an Agilent 1290 UHPLC system (Agilent) coupled to a TripleTOF 6600 mass spectrometer (Sciex). Chromatographic separation was achieved by gradient elution using a solvent system of 60:40 v/v acetonitrile/water (A) and 90:10 v/v isopropanol: water

(B), both containing 10mM ammonium formate and 0.1% formic acid. We used a 2.1 mm × 75 mm x 1.7μm CSH-C18 column (Waters, Eschborn, Germany) equipped with a 0.2μm in-line filter. Electrospray ionization was carried out in positive mode (ESI+) at an ion source temperature of 320°C and capillary voltage of 5500V. Full-scan MS data were acquired in an m/z range of 100–1650 at a scan rate of 4s-1. MS/MS spectra were 14 recorded in data-dependent mode auto-selecting the four highest m/z feature per peak (DDA Top-4 mode). Mass calibration was performed at the beginning of the sequence using an ESI (+) tune mix. For data analysis, MS files were converted to centroid mzML format using ProteoWizard and imported into MS-DIAL (Tsugawa et al., 2015). After data processing results were further analyzed using an R-script. Peak intensities were finally normalized and corrected for batch effects as described (Jaeger and Lisec, 2018).

Bioinformatics data analysis

The amount of lipid measured was normalized to the total lipid amount in samples and log-transformed to achieve asymmetric and approximatively normal distribution (Salatzki et al., 2018). Among many samples, lipid species with missing values were removed from the analysis. Normal distribution was checked visually by using Q-Q plots (Salatzki et al., 2018). Results are given in proportions, mean, standard deviation or standard error of the median with 25%–75% quartiles depending on their scale and distribution (Salatzki et al., 2018). Statistical tests for significance were performed by using the two-tailed t test or Mann-Whitney-U-test as appropriate (Salatzki et al., 2018). For class level comparisons only, regression or median imputation of missing values was used. A t test was used to detect differentially modulated lipid species. Vertical lines in the histograms indicate means ± standard error of the mean (SEM). Statistical significance was assumed at $p < 0.05$. The n-number is indicated for each experiment. All analysis were perfomed with R version 3.3.1. All analysis was conducted in collaboration with Kajetan Bentele, Yoann Gloaguen, and Dieter Beule from the Bioinformatic Core Unit of the Berlin Institute of Health (BIH).

Quantitative reverse transcription PCR (qRT-PCR)

Total RNA was extracted from isolated PCMs using RNeasy Micro Kit (Qiagen). All steps were performed according to the manufacturer's protocol. Prior to isolation, all equipment, and working area were disinfected with RNaseZAP (Sigma) to ensure deactivation of RNAses. mRNA analysis was performed as previously described (Salatzki et al., 2018). See Table S3 for primer sequences. PCMs were lysed with 150 μl RLT Lysis buffer supplied with β-Mercaptoethanol solution and transferred into QIAshredder SpinColumn and centrifuged for 2 min at RT at speed of 13,000 rpm. The supernatant was transferred into a new 1.5 ml Eppendorf tube and 295 μl RNA free water and 5 μl Proteinase K were added. The samples were then incubated for 10 min at 55°C, and afterwards centrifuged for 3 min at RT at a speed of 11000 rpm. The liquid fraction was isolated from the samples and mixed with 70% ethanol and applied on the silica-gel-based membrane columns (RNeasy-MinElute-Spin-Filter membrane, Qiagen). After a series of washing steps with 350 μl RW1-buffer, DNase was used to remove genome DNA from the RNA sample. Following 1 15 min incubation, DNase as well as other contaminants were washed away. The total purified RNA was eluted with 14 μ RNase-free water and incubated for 2 min at RT. Finally, RNA was stored at −80°C. RNA quantity and quality were analyzed by Nano drop. Reverse transcription was carried out using 1μl of total purified mRNA. Gene expression levels were assessed using qRT-PCR technique. cDNA was analyzed in the presence of the fluorescent dye (SYBRgreen). For the analysis, 4 μl cDNA (20ng) was used for the reaction. Relative expression of mRNA of the following genes: mmCLS, mmUCP2, mmUCP3, was calculated with the 2-ddct method (Livak and Schmittgen, 2001) after normalization the housekeeping gene mm18s. (see Table S3 for primer sequences).

Seahorse experiments (PCMs)

The bioenergetics response of PCMs was measured with the Seahorse XFe96 Analyzer following the manufacturer's instructions (Agilent, CA, USA). The XFe96 flux analyzer measures oxygen consumption rate (OCR) as a surrogate for mitochondrial oxidative phosphorylation activity and the ECAR, as a surrogate of lactate production. The XFe96 Analyzer monitors fluctuations in the oxygen levels over time and then calculates the rates of oxygen consumed known as OCR. Prior to plating, Seahorse XF96 cell culture plates were coated with 20μg/ml laminin (Thermo Fisher Scientific, MA, USA) for 2h at 37°C. Following isolation, PCMs were seeded at a population density of 4000/well in 100μl of media and allowed to adhere and grow in a 37°C humidified incubator with 5% CO2. The Cell mitochondrial stress test allows to assess key parameters of mitochondrial function in cells: basal respiration, ATP production, proton (H+) leak, maximal respiration, spare respiratory capacity, and non-mitochondrial respiration by application of oligomycin (2μM),

FCCP (0.3μM), and rotenone (1μM)/antimycin-A (1μM) (R/A). On completion of the XF assay, cells were lysed with lysis buffer reagent (30μl/well) and the protein concentration was determined using the BCA protein assay. OCR and ECAR data are expressed as pM/min/μg protein.

TBARS-assay

MDA is a product of lipid peroxidation and an indicator of oxidative stress in cells and tissues. Lipid peroxidation was estimated using the Thiobarbituric Acid Reactive Substances (TBARS) assay kit following the manufacturer's instructions (Cayman Chemical, MI, USA). Blood samples were collected immediately after excision of the mouse hearts and plasma was extracted. 50μl of sample or standard was added into 1.5ml Eppendorf, added to that 50μl of tricarboxylic acid assay reagent (10%), and 400μl of the color reagent. Samples were then heated at 95°C for 1h. Later, samples were immediately transferred on ice for 10min. Afterwards, samples were centrifuged for 10min at 1600g at 4°C. Lastly, 200μl from the samples (in duplicate) were carefully loaded into a colorimetric 96-well plate. Absorbance was read at 530-540nm using an ELISA plate reader.

Drosophila stocks and intravital heart parameters

Drosophila melanogaster were raised at room temperature in a 12h light-dark cycle receiving standardized food (Formula 4-24®, Carolina, NC, USA). All *Drosophila* strains used in this study are outlined in the key resources table. For experiments, three-week-old male flies were used. The heartbeat analysis and the assessment of cardiac functional parameters was performed using an adapted protocol for high-resolution fluorescence imaging of the *Drosophila* heart in unanesthetized whole flies, recently described by Klassen and colleagues (Klassen et al., 2017). Prior to analysis, flies were anesthetized using Fly Nap® (Carolina, NC, USA) and were fixated on a coverslip using Norland Optical adhesive #61 (Norland Products, NJ, USA), a clear, colorless, liquid photopolymer, that will cure after a 50s exposition to UV-light (MP38 Beurer GmbH, Ulm, Germany). After a 15min recovery period, imaging was performed in awake flies using a modified Leica DM6B fluorescent microscope and a digital CMOS camera (ORCA-Flash 4.0 V2, Hamamatsu, Japan). Fly hearts were imaged for 5s at 250 frames/s with 555nm illumination. All *Drosophila* heart data shown in the manuscript utilized the transgenic heart marker, *R94C02::tdTomato[attP40]* as heterozygotes (Klassen et al., 2017). For automated heartbeat 16 digitization of high-speed heart movies and their analysis we used a custom R script (https://github.com/graukatze/FlyHearts-tdtK-Rscripts). In brief, the walls of the adult heart tube were traced to return heart wall displacement over time. Individual beats were identified and automatically segmented into discrete contraction and relaxation events. Multiple morphological and functional spatiotemporal parameters were calculated from the segmented heartbeat waveforms including: end-diastolic and end-systolic diameter, fractional shortening, systolic and diastolic interval, heart period, maximum speed of contraction and relaxation, and the arrhythmia index of the heart period (Figure 3A) (Klassen et al., 2017). All graphs were generated in GraphPad Prism 6.

Seahorse experiments (Drosophila hearts)

To determine oxygen consumption in Drosophila hearts preparation of the heart was done first using the technique of semi-intact heart dissection (Blumrich et al., 2021; Fink et al., 2009). Flies were anaesthetized using FlyNap®. To access the heart tube of the fly, its head, ventral nerve cord, ventral abdominal cuticle, internal organs were carefully removed. Next, the entire fat body surrounding the fly heart was removed by careful suction. Finally, the thorax was removed completely and the beating fly heart on the abdominal cuticle remained. Each sample was transferred onto a XF96 microplate (Agilent). Vaseline was used to keep the samples attached to the bottom of the well. Restraints were placed on each sample to keep it in position during the measurement (Neville et al., 2018). While the dissection took place in artificial hemolymph (Singleton and Woodruff, 1994; Wang et al., 2003), the measurement of oxygen consumption was performed in 175 μl DMEM (including 2mM glucose, 2mM L-glutamine, Albumax® 1mg/ml, pH 7,4). Oxygen consumption measurement was performed using the Seahorse XFe96 Analyzer (Agilent). Using the following inhibitors, the different components of mitochondrial respiration could be addressed: Oligomycin (10 μM), Carbonyl Cyanide-p-trifluoromethoxyphenylhydrazone /FCCP (5 μM), antimycin A (2,5 μM) and rotenone (2,5 μM) (Sigma Aldrich).

Human myocardial specimens

Myocardial specimens from HFrEF patients and control subjects were from a tissue bank at the University Hospital Jena, Germany/ Columbia University, NY, USA. Samples from HFrEF patients with end-stage heart

failure were collected at the time of LV assist device-implantation, as previously described (Ji et al., 2017). Control samples were from deidentified specimens collected from non-failing hearts that were determined unusable for cardiac transplantation (Ji et al., 2017). Samples were immediately snap-frozen, placed in liquid nitrogen, and stored at −80°C until analysis.

Study approval

All animal experiments were performed in accordance with the guidelines of the German Law on the Protection of Animals and were approved by the Landesamt für Gesundheit und Soziales (LAGeSo), Berlin, Germany. All human studies were performed in accordance with the Declaration of Helsinki principles and were approved by internal review boards of the University Hospital Jena, Germany/Columbia University, NY, USA.

QUANTIFICATION AND STATISTICAL ANALYSIS

To compare differences between groups of PCMs or Drosophila, we performed two-way ANOVA with Bonferroni posttest, two-way ANOVA with repeated measures and Bonferroni posttest or ttest, as appropriate. The bioinformatic analysis of MS-based lipidomic data has been described above. Lipid amounts were normalized to total lipid amount in samples and log transformed (Salatzki et al., 2018). Depending on their scale and distribution, results are given in proportions, mean, median with 25%–75% quartiles, standard deviation, or standard error, as indicated. Statistical tests for significance were performed by using a t test or Mann-Whitney-U-test, as appropriate. Analyses were performed with R and Graph Pad Prism 6. Statistical significance 17 was assumed at $*p < 0.05$. All figure legends indicate the used statistical test, the n-number, and p value under each experiment.